Electrostatics for Exploring the Nature of Water Adsorption on the Laponite Sheets' Surface

Yosslen Aray,*,†,‡ Manuel Marquez,‡,§,||,⊥ Jesus Rodríguez,† Santiago Coll,† Yamil Simón-Manso,‡ Carlos Gonzalez,‡ and David A. Weitz||

Centro de Quimica, IVIC, Apartado 21827, Caracas 1020 A, Venezuela, Physical and Chemical Properties Division, National Institute of Standard and Technology (NIST), Gaithersburg, Maryland 20899, The Nanotechnology Lab, Kraft Foods R&D, 801 Waukegan Road, Glenview, Illinois 60025, Department of Physics and DEAS, Harvard University, 29 Oxford Street, Cambridge, Massachusetts 02138, and Los Alamos National Laboratory, Chemistry Division, Los Alamos, New Mexico 87545

Received: February 19, 2003; In Final Form: May 9, 2003

In this work, the topology of the electrostatic potential using density functional theory for periodic systems was used to study the nature of the interaction of water with laponite surfaces; an uncharged sheet model was also used. The topological analysis predicts that for uncharged surfaces the adsorption mode is such that the water molecules are adsorbed almost parallel to the surface. For laponite surfaces, where there is a net charge, the adsorption mode involves electrostatic repulsion between the negative lone pairs on the water molecules and the ones on the surface oxygen atoms. As a consequence, the water molecules bind to the surface in a perpendicular and tilted approach, minimizing the repulsive interactions. The advantage of using the topology of the electrostatic potential as an efficient method to describe the electrostatic interactions between adsorbates and surfaces is also discussed.

Introduction

"Smart" gels are a class of materials that expand and/or contract as a result of changes in temperature, pH, solvent polarity, light, or any other external stimulus.[1] The relatively low cost involved in their fabrication, combined with their ability to undergo significant but reversible changes in volume as a response to an external stimulus, makes these materials the perfect vehicle to encapsulate and release other materials in a very cost-effective manner. The range of technological and industrial applications of smart gels is quite large, and it widens in scope every day. They can be used in the generation of powerful sensors and actuators on the nanoscale level and in molecular filters and molecular recovery systems. Among the different kinds of smart gels currently under development, "shake" gels (SG) have attracted considerable interest in industry. Shake gels[2] are formed by aqueous solutions of synthetic clays and polymers that form a gel after the solution is shaken. The most common SG is built from mixtures of laponite, poly(ethylene oxide) (PEO), and water. These materials form a clear solution that leads to a gel once shaken. This gel relaxes back to a liquid after a certain period of time that depends on the laponite and PEO concentrations. At longer times, the mixture forms a permanent gel because of an aging process that is not well understood. Despite the considerable interest in the properties of these materials, the design and synthesis of SGs have relied on an empirical approach that entails long and expensive trial-and-error experimental procedures. Fundamental questions dealing with the nature of the interactions between the components that lead to gel formation after shaking need to be answered to pave the way for the rational design of these materials. Simulations of these systems based on reliable theoretical methodologies offer a powerful tool that can complement the experimental data in order to shed some light on the mechanisms governing the formation and stability of shake gels. Water−PEO−laponite is a complicated system that entails a competition between the PEO and water binding to the clay. To understand the net effects of these interactions in the actual system, it is useful to understand each individual one. Thus, as part of an ongoing systematic study dealing with the nature of these interactions, in this work we present the results of theoretical calculations describing the binding between water and laponite.

A molecular-level understanding of the adsorption of water on the surfaces of clay particles is of fundamental importance to many processes.[3−6] Clean, chemistry-customized synthetic clays have made a large variety of useful and interesting experimental and theoretical model systems[3,7] accessible. The most widely studied synthetic clay to date is laponite,[3,7] a synthetic clay whose composition is on average $[Mg_{5.25}Li_{0.75}]$-$Si_8O_{20}(OH)4Na_{0.75}$ and belongs to the family of so-called swelling 2:1 smectites. The behavior of water adjacent to a variety of clay surfaces has been studied using different experimental[8−12] and computational techniques.[13−18] It is generally concluded that the clay equilibrium hydration state is related to the magnitude and localization of the clay layer charge. Monte Carlo[13] and molecular dynamics[15,16] studies of water molecules at uncharged clay surfaces of talc and kaolinite have found that the water molecules are adsorbed in the center of the SiO_2 surface ring, each oriented with its molecular HOH plane approximately parallel to the clay surface. It was suggested[13] that in each ring a hydrogen bond involving the internal hydroxyl

* Corresponding author. E-mail: yosslen.aray@nist.gov. Fax: (+58) 212 504 1350.
† Centro de Quimica.
‡ National Institute of Standard and Technologies.
§ Kraft Foods R&D.
|| Harvard University.
⊥ Los Alamos National Laboratory.

10.1021/jp0302257 CCC: $25.00
Published on Web 07/24/2003

groups of the clay is formed. High-resolution neutron diffraction studies[8,9] and Monte Carlo simulations[20] of water confined between the charged layers of natural vermiculite clays have shown that two ordered layers of water molecules are observed close to the clay sheets. A Monte Carlo and a molecular dynamics simulation[17] of the structure and dynamics of the interlayer aqueous solution in colloidal sodium laponite clay have clearly shown that the water structure near the clay surface is significantly perturbed compared to the water structure in the pure condensed phase. Similar to the vermiculite clays, two ordered layers of water were observed close to the clay sheets. The first layer of water is tilted and strongly oriented to form hydrogen bonds to the surface oxygen atoms at a distance of 1.85 Å from the surface. Despite the amount of experimental and theoretical work in this area, the origin and nature of this behavior remain elusive.

The topographic features of the electrostatic potential $V(\mathbf{r})$ of molecules are particularly useful for understanding the hydration process.[21−25] $V(\mathbf{r})$ at a point $\mathbf{r}$ generated by a molecule is given by

$$V(\mathbf{r}) = V_{\mathrm{N}}(\mathbf{r}) + V_{\mathrm{E}}(\mathbf{r}) \tag{1}$$

where the two terms represent the bare nuclear and electronic contributions, respectively, to the total electrostatic potential. The sign of $V(\mathbf{r})$ at a given point indicates whether the nuclear or electronic effects are dominant. The topological properties of $V(\mathbf{r})$ are summarized by its critical points (CP). These are points where the gradient vector field, $\nabla V(\mathbf{r})$, vanishes, and they are classified by the $V(\mathbf{r})$ curvature or three eigenvalues λ_i (i =1, 2, and 3) of the corresponding Hessian matrix ($\mathbf{H}_{ij} = \partial^2 V(\mathbf{r})/\partial x_i\, \partial x_j$). In molecules and crystals, there are four types of these extremes that are labeled by their rank (number of nonzero eigenvalues) and signature (excess number of positive vs negative eigenvalues). These can be maxima (3, −3), minima (3, +3), or (3, −1) and (3, +1) saddles that bridge either two minima or two maxima. For the region closest to the nucleus, V_{N} dominates, and $V(\mathbf{r})$ has exactly the same topology of electron density, $\rho(\mathbf{r})$ [26] (i.e., positive-valued maxima at the nuclear site and a positive-valued (3, −1) bond saddle between every pair of bonded atoms). For the region where V_{E} dominates ($V(\mathbf{r}) < 0$), the EP topography can be more complex. However, it is well known that lone pairs of electrons as well as double π bonds (C═C, C═N, etc.) are generally characterized as negative valued (3, +3) minima.[24,25] By locating CPs in electrostatic potentials, one can precisely identify the host sites in which water molecules bind. Thus, the positive-valued EP zone of the hydrogen atoms in the water molecules are positioned over the minima of the negative EP zone of the substrate.[24,25]

In this work, the nature of the interaction of water molecules with the surface of the laponite sheets has been studied by carrying out a systematic determination of the topology of $V(\mathbf{r})$ for the laponite platelet surface, water molecules, and an uncharged sheet model using ab initio density functional theory (DFT) methods for periodic systems. It is shown that the computation of the topology of $V(\mathbf{r})$ provides a reliable and relatively inexpensive method (that does not require the full-geometry optimizations of the supermolecule) of studying the nature of the interactions between adsorbates and extended surfaces. To our knowledge, this novel methodology has not been previously used to treat these systems.

Computational Methodology

The electrostatic potential at $\mathbf{r}$ generated by the total charge distribution, ρ^{tot}, of a periodic system is given by[27]

$$V(\mathbf{r}) = \sum_n \int \rho^{\mathrm{tot}}(\mathbf{r}' - \mathbf{R}_n)|\mathbf{r} - \mathbf{r}'|^{-1}\, \mathrm{d}\mathbf{r}' \tag{2}$$

The summation extends to all direct lattice vectors, the prime on the integral sign indicating that an infinitesimal region about $\mathbf{r} = \mathbf{r}'$ is excluded from the domain of integration to avoid divergent nuclear self-interaction terms that would otherwise arise in the electrostatic energy per cell.[27] ρ^{tot} may be decomposed into electronic and nuclear components

$$\rho^{\mathrm{nuc}}(\mathbf{r}) = \sum_a q_a\, \delta(\mathbf{r}_a, \mathbf{r}) \tag{3}$$

where the summation extends to all of the reference cell nuclei, with atomic numbers and position vectors denoted q_a and $\mathbf{r}_a$, respectively.

$$\rho^{\mathrm{el}}(\mathbf{r}) = -\sum_{ij}\sum_{\mu\nu} \mathbf{P}_{\mu\mathbf{R}_i\nu\mathbf{R}_j} \chi_\mu(\mathbf{r} - \mathbf{R}_i)\, \chi_\nu{}^*(\mathbf{r} - \mathbf{R}_i) \tag{4}$$

where $\mathbf{P}$ is the density matrix and $\chi_\mu(\mathbf{r} - \mathbf{R}_i)$ is the μth reference cell local Gaussian basis function translated by the direct lattice vector $\mathbf{R}_i$. The summation over i and j extend to all direct lattice vectors, and those over μ and ν include all of the basis functions of the reference cell. Substituting eqs 3 and 4 into eq 2 gives the nuclear and electronic $V(\mathbf{r})$ contributions.

For the studied systems, $V(\mathbf{r})$ was calculated by means of the CRYSTAL98[28,29] program using the Khon−Sham Hamiltonian with the gradient-corrected Perdew−Becke−Ernzerhof (PBE) exchange potential.[30] For the laponite surface, 66-21G*, 6-21G*, and 86-21G* Gaussian basis sets for Si, O, and Mg[31] and 6-21G* for the H[31] atoms was used. In addition, a 6-21G**[32] basis was used for the water molecules.

The topology of $V(\mathbf{r})$ was analyzed using an algorithm developed in our laboratory in the same way that those developed for the study of electronic density topology[33,34] were used. The CPs were calculated using the Newton−Raphson (NR) technique.[35] The NR algorithm starts from a truncated Taylor expansion at a point $\mathbf{r} = \mathbf{r}_0 + \mathbf{h}$ about $\mathbf{r}_0$ of a multidimensional scalar function ($\nabla V(\mathbf{r})$):

$$\nabla V(\mathbf{r}) = \nabla V(\mathbf{r}_0) + \mathbf{H}_0\mathbf{h} + \text{higher-order terms} \tag{5}$$

where $\mathbf{H}$ is the Hessian (the Jacobian of $\nabla V(\mathbf{r})$) at point $\mathbf{r}_0$. Given that a CP is characterized by $\nabla V(\mathbf{r}) = 0$, the optimal step $\mathbf{h}$ is then given by $\mathbf{h} = -\mathbf{H}^{-1}\nabla V(\mathbf{r}_0)$. This second-order correction is then used to obtain a vector $\mathbf{r}_{\mathrm{new}} = \mathbf{r}_{\mathrm{old}} + t\mathbf{h}$ (t is a small value), and the process is iterated to $\nabla V(\mathbf{r}) = 0$. The NR algorithm requires the evaluation of the first $\{V'\}$ and second $\{V''\}$ partial derivatives of $V(\mathbf{r})$ at arbitrary points $\mathbf{r}$. These partial derivatives are evaluated by numerical differences and are fed into an automated algorithm for the systematic determination of the all of the CPs inside the unit cell of the crystal.[33,34]

Model of Idealized Laponite Sheets. All dehydrated smectites consist of a layered silicate microstructure where each mineral leaf is a monocrystalline structure consisting of 2D sheets of tetrahedral silica $(SiO_4)^{-2}$ covalently bonded together.[3,7] In laponite, the octahedral sites between the tetrahedral sheets are occupied by Mg (or Li) ions. The 2:1 clays in general consist of charged 1-nm-thick sheets, which in the dry state stack by sharing charge-compensating cations. Under hydration, laponite forms suspensions of 25-nm-diameter colloidal platelets. Water can easily penetrate the interleaf regions, dissolving the interleaf cations and separating the platelet surfaces by solvation forces. In dilute suspensions, the platelets separate completely

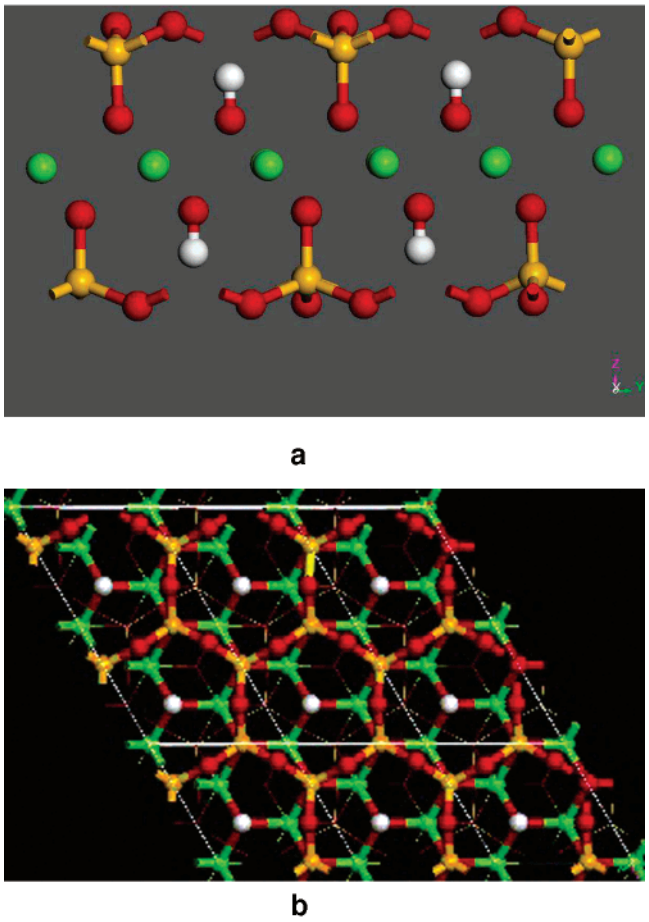

Figure 1. Structure of the unit cell of the idealized laponite platelet. (a) Side view of a 1 × 1 cell. (b) Top view of a 3 × 3 cell. Red, yellow, green, and white spheres denote O, Si, Mg, and H atoms, respectively.

and become dispersed as colloidal platelets, and the sodium cations diffuse into the surrounding polar liquid and screen the negative surface charge. These platelets may be individually considered to be single particles with a well-defined crystal structure.[3,7]

Laponite is a typical synthetic smectite that resembles the natural clay hectorite in structure and composition. The hectorite[36] lattice is a monoclinic-prismatic cell described by the space group $C2/m$ with parameters $a = 5.25$ Å, $b = 9.18$ Å, $c = 16.0$ Å, $\alpha = 90°$, $\beta = 99°$, and $\gamma = 90.0°$. The unit cell of the platelet is constructed of a single octahedral sheet sandwiched between two tetrahedral layers, with the octahedral sheet sharing the apical oxygen of the tetrahedral layer (Figure 1). This structure has a neutral charge: there are 6 octahedral magnesium ions, 2 layers of 4 tetrahedral silicon atoms, 20 oxygen atoms, and 4 hydroxyl groups. Each layer of the ideal platelet consists of a hexagonal network of basal oxygen atoms of the tetrahedral Si−O. We have built the model of an uncharged ideal platelet by leaving a sheet of the hectorite cell parallel to the (001) plane. Vacuum layers thicker than 10 Å were used to ensure that there were no interactions between adjacent slabs. The symmetry of the cell changes from monoclinic to a triclinic type P-1. The geometry of the cell was fully optimized using the Castep program,[37] fixing the c parameter at 20.0 Å. In this program, the Kohn−Sham equations of DFT are variationally solved in a plane-wave basis set using optimized ultrasoft pseudopotentials in Kleinman−Bylander form[38] for the description of the electron−ion interactions. The exchange-correlation part of the Hamiltonian is described using the generalized gradient approximation of Perdew−Burke−Ernzerhof.[30] A conjugate gradients minimization scheme is utilized to locate the electronic ground states directly. The calculation of the Hellmann−Feynman forces acting on the atoms and a standard BFGS technique allows the structural optimization to be carried out. The optimized parameters were $a = b = 5.26$ Å, $\alpha = \beta = 90°$, and $\gamma = 120°$. Figure 1b shows the top view of a 3 × 3 supercell. A 25-nm-diameter platelet contains about a 50 × 50 supercell.

TABLE 1: Topological Properties (au) of $V(\mathbf{r})$ at the Critical Points (CP) for the H_2O Molecule

CP	λ_1	λ_2	λ_3	$V(\mathbf{r}_c)$
minima (3, +3) 2 oxygen lone pairs	0.0017	0.0383	0.1900	−0.1043
1 saddle (3 + 1)	−0.0009	0.0372	0.1872	−0.1042
2 (3, −1) OH bonds	−4.387	−4.180	13.259	1.1464

TABLE 2: Topological Properties (au) of $V(\mathbf{r})$ at the Critical Points (CP) for the Outermost SiO Ring of the Uncharged Platelet Surface

CP	λ_1	λ_2	λ_3	$V(\mathbf{r}_c)$
6 minima (3, +3) at the oxygen atoms	0.0019	0.0294	0.0722	−0.0946
6 saddle (3 + 1)	−0.0044	0.0015	0.0040	−0.0295
12 (3, −1) SiO bonds	−1.2885	−1.2789	5.4419	0.8078

In the real systems, some of the magnesium atoms are substituted by lithium ions, and some spaces are empty, giving the corresponding empirical formula $Na^{+}_{0.7}[Si_8Mg_{5.5}Li_{0.3})O_{20}(OH)_4]^{-0.7}$. Laponite leads to platelets with a layer charge of $-0.75e$ per unit cell. The model of the charged platelet was built in a similar way (i.e., by leaving a sheet of the hectorite cell parallel to the (001) plane). To obtain the overall negative charge closest to the empirical formula, the substitution of one Li for a Mg atom was carried. This site was selected to lie as far away as possible, thereby producing a mostly regular array of lithium atoms. The starting configuration was prepared by placing a sodium counterion at the middle of the SiO ring and $^{c}/_{2}$ Å from the surface. This cell was replicated through a point of inversion at the origin and converted to a P-1 unit. The resulting unit cell is shown in Figure 2. The geometry of the cell was also fully optimized using the CASTEP program, fixing the c parameter of the cell at 30.0 Å. The optimized parameters were $a = 10.584$ Å, $b = 9.166$ Å, and $\alpha = \beta = \gamma = 90°$.

Results

Interactions between Water and the Uncharged Surface. The $V(\mathbf{r})$ topological features of the isolated water molecule are shown in Figure 3, and the corresponding CP properties are listed in Table 1. As previously reported,[23] the negative potential is located over the nonbonding region of the oxygen atom forming a lone-pair pattern with two negative-valued minima connected by a (3, +1) saddle point. The EP over the entire nuclear region is positive with a (3, −1) CP associated with each OH bond.

The corresponding topological features of a ring of the uncharged platelet surface are shown in Figure 4, and the parameters that characterize the obtained CPs are collected in Table 2. The EP negative region is localized outside the surface over the nonbonding region of the oxygen atoms, and the EP over the entire ring region is positive. Figure 4b clearly shows that the negative EP zone is exposed to the incoming molecules and that it hinders free access to the positive area of the surface. There is a set of six minima, located only at the oxygen site,

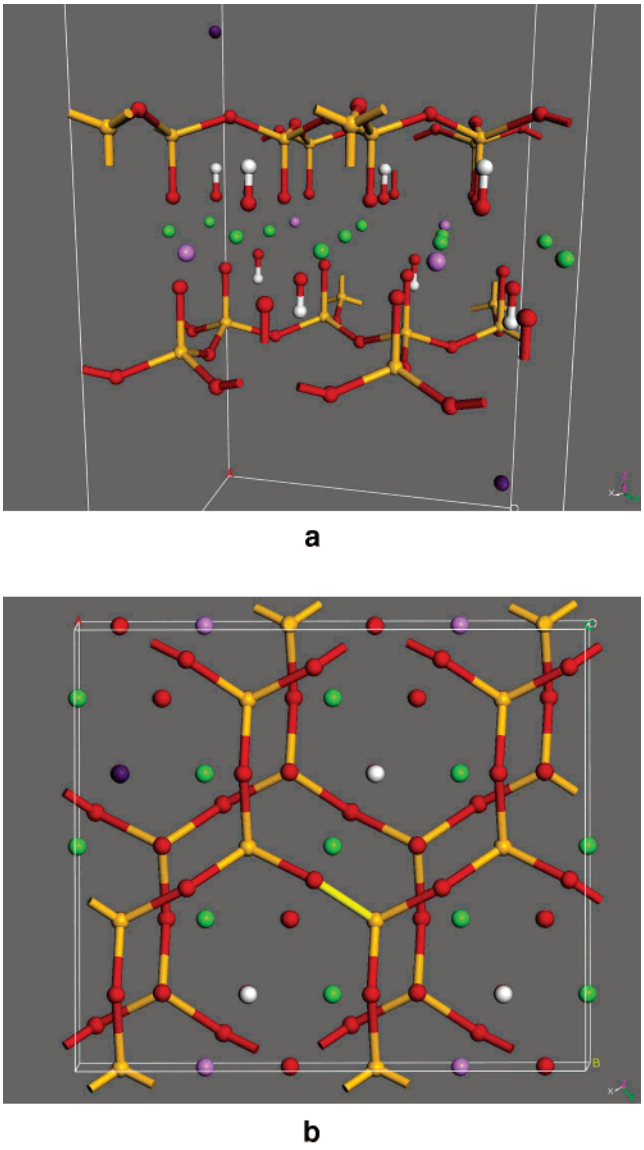

Figure 2. (a) Side view and (b) top view of the optimized unit cell of the laponite platelet. Red, yellow, green, white, pink, and dark-blue spheres denote O, Si, Mg, H, Li, and Na atoms, respectively.

connected by a set of six (3, +1) saddle points on the negative zone and, as expected, a positive (3, −1) saddle at each Si−O bond.

The topological properties of the isolated water molecule and uncharged surface discussed above lead to the conclusion that water molecules can bind to the surface only by the mode shown in Figure 5, which is driven by mutual alignment of the water hydrogen atoms to adjacent minima of two surface oxygen atoms and one water lone pair (minimum) that points toward the positive zone at a Si atom.

To test the validity of the predictions made by the EP model, the binding of the water molecule on the uncharged surface was explored using the CASTEP program.[37] A monolayer of water molecules (one per cell) was placed inside the surface cell, and the system was completely optimized while the cell parameters were fixed. A top view of the optimized adsorption mode is shown in Figure 6: the H_2O molecules are adsorbed almost parallel to the surface, centered at each ring, with $H-O_{surfaces}$, $O_{water}-Si_{surface}$, and $O_{water}-O_{hydroxyl}$ distances of 2.477, 3.599, and 2.657 Å, respectively. These results are in excellent agreement with the predictions of our EP model and experimental and theoretical data available in the literature.[13,15,16] The

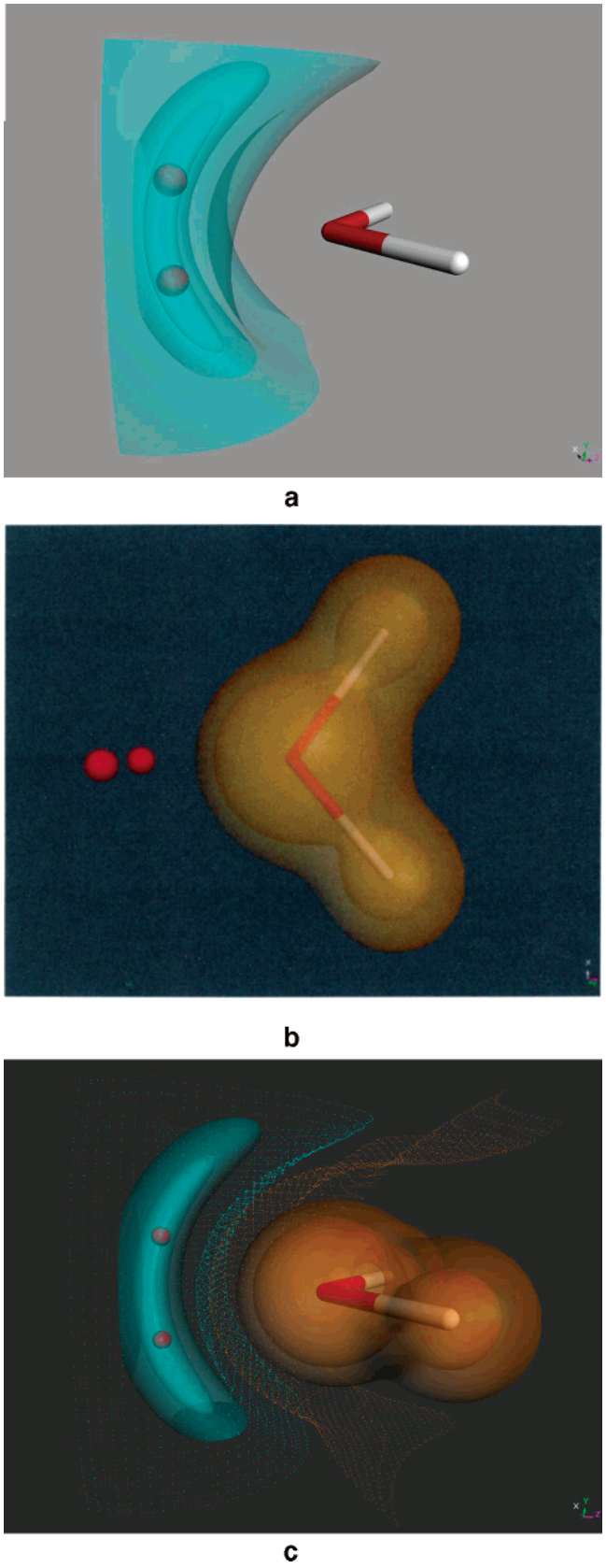

Figure 3. Contour maps of the electrostatic potential (EP) for the H_2O molecule. Blue and yellow zones denote the negative and positive values of the EP, respectively. (a) Side view of the negative-valued zone. (b) Top view of the positive-valued zone. Red spheres denote the EP minima critical points characterizing the oxygen lone pairs. Red and white cylinders denote O and H atoms, respectively. (c) Complete view of the H_2O EP. Dotted contours denote the border of the region.

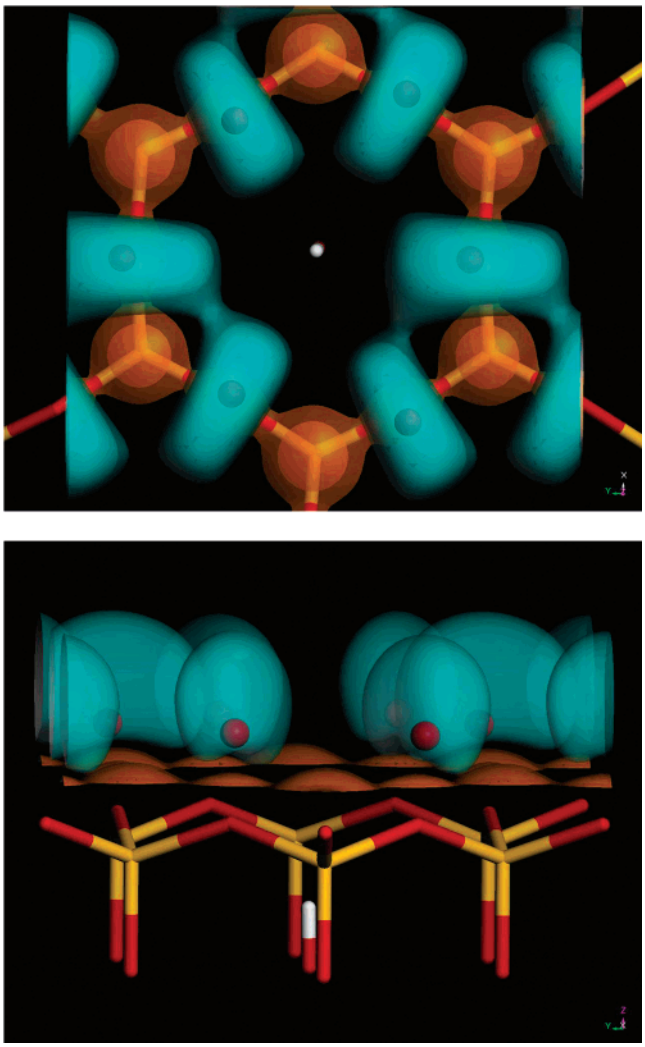

Figure 4. Top and side views of the contour maps of EP for a ring of the uncharged platelet surface. Yellow and red cylinders denote Si and O atoms, respectively. Blue and yellow zones denote negative (around the O atoms) and positive values of the EP, respectively. Red spheres denote the EP minima critical points on the negative zone of the potential. The negative area impedes the easy access to the positive area of the surface.

binding energy (BE) of this configuration was found to be 10.79 kJ mol^{-1} per cell. This BE was calculated by the following expression:

$$\mathrm{BE} = E_{\mathrm{S-W}} - E_{\mathrm{S}} - E_{\mathrm{W}} \tag{6}$$

with $E_{\mathrm{S-W}}$ = total energy of the H_2O monolayer adsorbed on the surface, E_{S} = total energy of the isolated surface, and E_{W} = total energy of the H_2O layer isolated in the cell.

Interactions between Water and the Laponite Surface. Given the excellent qualitative agreement between the EP model and the CASTEP calculations in describing the adsorption mode of water into the uncharged surface, we applied the same methodology to probe the interactions between water molecules and the laponite surface.

The EP topological features for the laponite surface are shown in Figure 7, and the parameters that characterize the calculated CPs are collected in Table 3. Figure 7 shows that the charge in the laponite unit cell produces drastic changes in the $V(\mathbf{r})$ topology as compared to the uncharged ideal surface model (Figure 4). It is observed that each outermost oxygen atom is characterized by two lone pairs (red spheres) lying along the

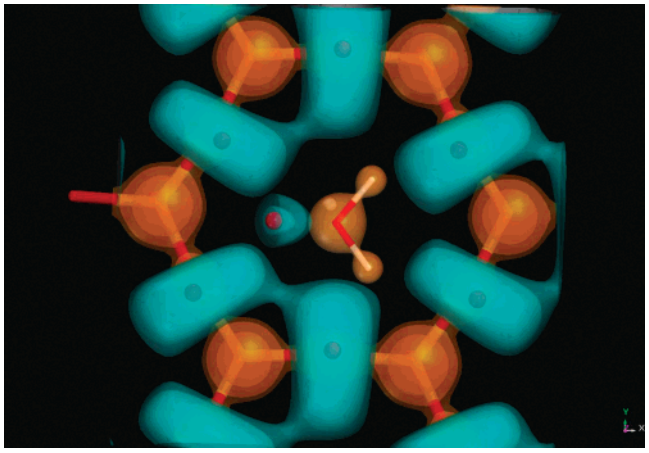

Figure 5. Top view of the predicted adsorption mode of the water molecule on a ring of the uncharged surface. Blue and yellow zones denote negative (around the O atoms) and positive values of the surface EP, respectively. Red spheres denote the oxygen EP minima critical points.

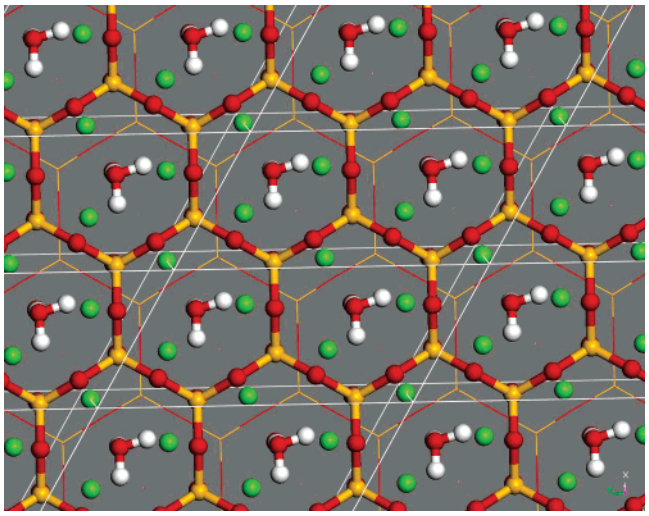

Figure 6. Top view of the optimized structure of a water monolayer on the uncharged clay platelet surface. Yellow, red, white, and green spheres denote Si, O, H, and Mg atoms, respectively.

nonbonding region of the negative potential (light blue). These lone pairs are located inside the rings and connected by a (3, +1) saddle point sitting on top of the oxygen atom. The net effect of the charge on the laponite is the concentration of the negative EP inside the ring and away from the Si atoms. Note that the value of $V(\mathbf{r})$ at the negative minima of the charged surface is 3 times the corresponding value for the uncharged surface (Table 3).

The EP topology for laponite leads to the conclusion that contrary to the ideal uncharged model system the water molecules bind to the surface in a perpendicular approach that finally yields different tilted arrangements such as the ones shown in Figure 8. These modes involve the attractive interactions between the positive zone around the H atoms of the water molecule and two negative minima lone pairs at neighbor surface oxygen atoms. One possible mode (Figure 8a) involves an additional attractive interaction of a water oxygen lone pair with the positive zone of a Si atom of the surface, and another mode (Figure 8b) involves electrostatic repulsion between the negative lone pairs on the water and the surface oxygen atoms. It is also possible that an entirely perpendicular mode exists, mainly dominated by the attractive interaction between the water hydrogen atoms and the oxygen atoms on the surface. As a

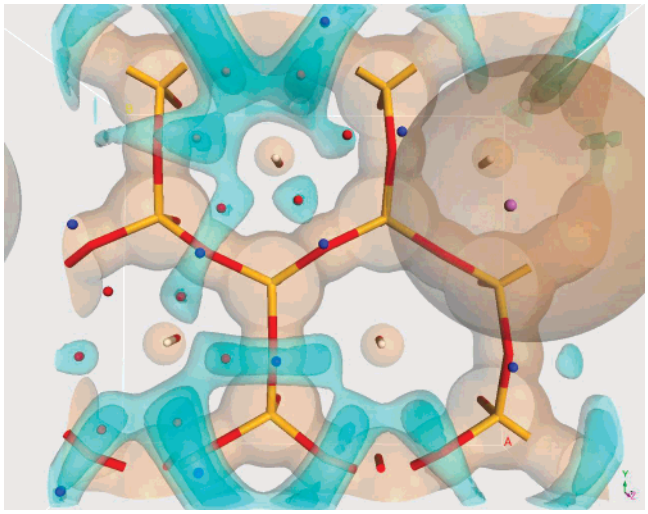

Figure 7. Top view of a contour map of the unit cell of the laponite platelet surface. Red, yellow, green, and white cylinders denote O, Si, Mg, and H atoms, respectively. Blue and yellow zones denote negative and positive values of the EP, respectively. Red and blue spheres denote EP minima and saddle critical points on the negative zone of the potential, respectively.

TABLE 3: Topological Properties (au) of Electrostatic Potential at the Critical Points, $V(\mathbf{r}_c)$, for One of the Outermost SiO Rings of the Laponite Platelet Surface

CP	λ_1	λ_2	λ_3	$V(\mathbf{r}_c)$
3 minima (3, +3) close to a Li atom	0.0178	0.0391	0.0898	−0.1067
3 minima (3, +3) far from a Li atom	0.0070	0.0372	0.1271	−0.1414
3 saddle (3 + 1) close to a Li atom	−0.0085	0.0345	0.2038	−0.0983
3 saddle (3+1)	−0.0038	0.0276	0.2093	−0.1217
4 (3, −1) SiO bonds near to a Li atom	−1.2734	−1.2655	5.4636	0.6643
8 (3, −1) SiO bonds far from a Li atom	−1.2878	−1.2690	5.5155	0.70145

consequence of the interactions described above, the water molecules should not be parallel to the surface. On the contrary, the water molecules should be perpendicular or tilted, maximizing the attractive interaction between the Si atoms and the H_2O lone pair and/or minimizing the repulsive interaction between the minima lone pairs of the water and surface oxygen atoms.

The results listed in Table 3 indicate that the oxygen lone-pair minima of the surface closest to the Mg atoms are deeper than those closest to the Li atoms. Consequetly, the EP topology predicts that the water molecules should prefer to adsorb in the vicinity of the surface oxygens located above the Mg atoms. Additionally, the values of $V(\mathbf{r})$ at the oxygen minima lone pairs indicate that the $H_{water}-O_{surface}$ bond must be stronger in the case of the laponite charged surface.

As with the uncharged surface case, full optimizations using the DFT module contained in the CASTEP program[16] were carried out to validate the predictions of the EP model. A monolayer of water molecules was placed inside the surface cell, and the system was optimized while the cell parameters were fixed. A top view of the optimized adsorption mode is shown in Figure 8c. In agreement with the EP topology analysis, the optimization results indicate that the H_2O molecules are adsorbed almost perpendicularly to the surface, nearly to the oxygen above the Mg atoms, with $H-O_{surface}$ and $O_{water}-O_{hydroxyl}$ distances of 2.441 and 3.402 Å, respectively. The adsorption modes predicted by our EP model and CASTEP calculations are in very good agreement with experimental[8,9] and computational[17,20] results previously reported in the literature. The calculated BE for this adsorption mode was 19.58 kJ

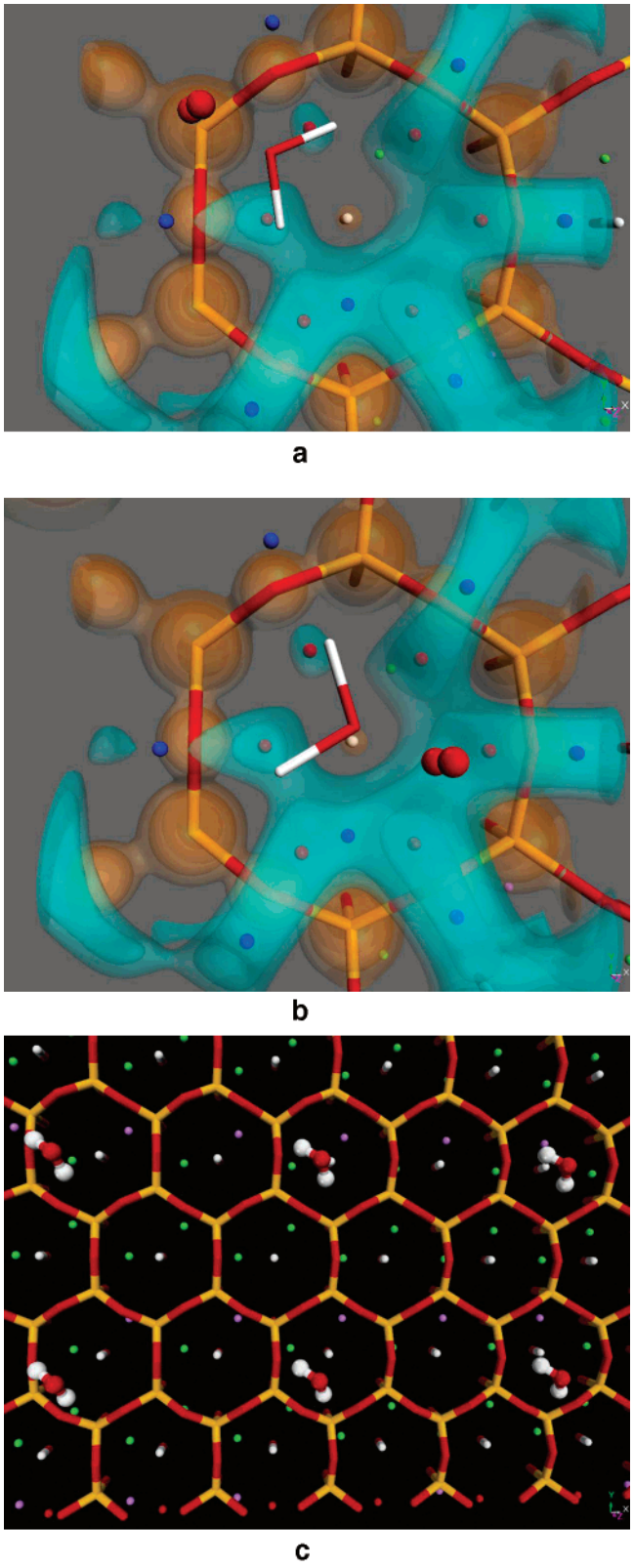

Figure 8. (a and b) Top view of the EP-predicted water adsorption modes on a ring of the laponite platelet surface. Blue and yellow zones denote negative and positive values of the EP, respectively. Red spheres denote EP minima critical points. Large red spheres denote lone-pair minima CPs of the water molecule. (c) Top view of a cylinder model showing the adsorption mode of a water (ball-and-stick models) monolayer on the laponite platelet surface. Yellow, red, green, violet, and white cylinders denote Si, O, Mg, Li, and H atoms, respectively.

mol^{-1} per cell, which is almost 100% larger than the corresponding value (10.79 kJ mol^{-1}) for the uncharged surface.

Final Remarks

The results obtained in this work indicate that the analysis of the EP topology of the isolated interacting systems (water and surface) provides a reliable and efficient method to predict and understand the different adsorption modes of complicated systems involving molecules and surfaces dominated by electrostatic interactions. In water−clay systems such as the ones studied in this work, the model provides a useful tool to understand the effect of charge in the system. As our results indicate, the presence of charge in the laponite surface drives the water adsorption toward perpendicular and tilted configurations, in stark contrast to the uncharged surface, where the only adsorption mode consist of water molecules lying parallel to the surface. We are currently extending our calculations to include polymer adsorption on hydrated clay surfaces, which is important in the design of shake gels.

References and Notes

(1) (a) Ilmain, F.; Tanaka, T.; Kokufuta, E. *Nature* **1991**, *349*, 6308. (b) Annaka, M.; Tanaka, T. *Nature* **1992**, *355*, 6359. (c) Pande, V. S.; Grosberg, A. Yu.; Tanaka, T. *Proc. Nat. Acad. Sci. U.S.A.* **1994**, *91*, 12976.

(2) (a) Zebrowski, J.; Prasad, V.; Zhang, W.; Walker, L. M.; Weitz, D. A.; *Colloids Surf., A* **2002**, *213*, 189. (b) www.deas.harvard.edu/projects/weitzlab/research/laponite.html.

(3) Fossum, J. O. *Physica A* **1999**, *270*, 270.

(4) Swenson, J.; Smalley, M. V.; Hatharashinge, H. L. M.; Fragneto, G. *Langmuir* **2001**, *17*, 3813.

(5) Kuppa, V.; Manias, E. *Chem. Mater.* **2002**, *14*, 2171.

(6) Lal, J.; Auvray, L. *J. Appl. Crystallogr.* **2000**, *33*, 673.

(7) Technical Bulletin. Southern Clay Products, 2001, www.scprod-.com/laponite/prod, www.laponite.com.

(8) Williams, G. D.; Soper, A. K.; Skipper, N. T.; Smalley, M. V. *J. Phys. Chem. B* **1998**, *102*, 8945.

(9) Swenson, J.; Smalley, M. V.; Thomas, R. K.; Crawford, R. J.; Braganza, L. F. *Langmuir* **1997**, *13*, 6654.

(10) Laird, D. A. *Clays Clay Miner.* **1999**, *47*, 630.

(11) Costanzo, P. M.; Giese, R. F.; Lipsicas, M. *Clays Clay Miner.* **1984**, *32*, 419.

(12) Sermon, P. A. *J. Chem. Soc., Faraday Trans. 1* **1980**, *76*, 885.

(13) Bridgeman, C. H.; Skipper, N. T. *J. Phys.: Condens. Matter* **1997**, *9*, 4081.

(14) Bridgeman, C. H.; Buchingham, A. D.; Skipper, N. T.; Payne, M. C. *Mol. Phys.* **1996**, *89*, 879.

(15) Warne, M. R.; Allan, N. L.; Cosgrove, T. *Phys. Chem. Chem. Phys.* **2000**, *2*, 3663.

(16) Smirnov, K. S.; Bougeard, D. *J. Phys. Chem. B* **1999**, *103*, 5266.

(17) Leote de Carvalho, R. J. F.; Skipper, N. T. *J. Chem. Phys.* **2001**, *114*, 3727.

(18) Delville, A. *J. Phys. Chem.* **1993**, *97*, 9703.

(19) Delville, A. *J. Phys. Chem.* **1995**, *99*, 2033.

(20) Skipper, N. T.; Refson, K.; McConnell, J. D. C. *J. Phys. Chem.* **1991**, *94*, 7434.

(21) *Chemical Applications of Atomic and Molecular Electrostatic Potentials: Reactivity, Structure, Scattering, and Energetics of Organic, Inorganic, and Biological Systems*; Politzer, P., Truhlar, D. G., Eds.; Plenum Press: New York, 1982.

(22) *Molecular Electrostatic Potential: Concepts and Applications*; Murray, J. S., Sen, K. D., Eds.; Elsevier: Amsterdam, 1996.

(23) Gadre, S. R.; Shirsat, R. N. *Electrostatics of Atoms and Molecules*;Universities Press: Hyderabad, India, 2000.

(24) Gadre, S. R.; Babu, K.; Rendell, A. P. *J. Phys. Chem. A* **2000**, *104*, 8976.

(25) Pingale, S. S.; Gadre, S. R.; Bartoli, L. J. *J. Phys. Chem. A* **1998**, *102*, 9987.

(26) Keith, T. A.; Bader, R. F. W.; Aray, Y. *Int. J. Quantum Chem.* **1996**, *183*, 183.

(27) Saunders, V. R.; Freyria-Fava, C.; Dovesi, R.; Salasco, L.; Roetti, C. *Mol. Phys.* **1992**, *77*, 629.

(28) Dovesi, R. *Phys. Status Solidi* **2000**, *217*, 63.

(29) Saunders, V. R.; Dovesi, R.; Roetti, C.; Causa, M.; Harrison, N. M.; Orlando, R.; Zicovich-Wilson, C. M. *CRYSTAL98 User's Manual*; University of Torino: Torino, Italy, 1998.

(30) Perdew, J. P.; Burke, K.; Ernzerhof, M. *Phys. Rev. Lett.* **1996**, *77*, 3865.

(31) Nada, R.; Catlow, C. R. A.; Dovesi, R.; Saunders, V. R. *Proc. R. Soc. London, Ser. A* **1992**, *436*, 499.

(32) Hehre, D. J.; Radom, L.; Schleyer, P. V. R.; J. Pople, A.; Aray, Y.; Rodriguez, J.; Lopez-Boada, R. *J. Phys. Chem.* **1997**, *101*, 2178.

(33) Aray, Y.; Rodriguez, J.; Vega, D. *Comput. Phys. Commun.* **2002**, *143*, 199.

(34) Press, W. H. *Numerical Recipes in FORTRAN: The Art of Scientific Computing*, 2nd ed.; Cambridge University Press: Cambridge, England, 1992; p 708.

(35) Newnam, A. C. D. *Chemistry of Clays and Clay Minerals*; Mineralogical Society: London, 1987.

(36) *CASTEP*, release 4.5. Accelerys Inc: San Diego, CA, 2001.

(37) Kleinman, L.; Bylander, D. M. *Phys. Rev. Lett.* **1982**, *48*, 1425.